Effect of mechanical depoling on piezoelectric properties of $Na_{0.5}Bi_{0.5}TiO_3$ - $xBaTiO_3$ in the morphotropic phase boundary region

Lyndsey M. Denis[1,2,7], Julia Glaum[3,4], Mark Hoffman[3], John E. Daniels[3], Ryan J. Hooper[1], Goknur Tutuncu[5], Jennifer S. Forrester[6], and Jacob L. Jones[5*]

[1]*Department of Materials Science and Engineering, University of Florida, Gainesville, Florida 32611, USA*

[2]*Department of Chemical Engineering, University of Florida, Gainesville, Florida 32611, USA*

[3]*School of Materials Science and Engineering, University of New South Wales, Sydney, New South Wales 2052, Australia*

[4]*Department of Materials Science and Engineering, Norwegian University of Science and Technology NTNU, Trondheim, 7491, Norway*

[5]*Department of Materials Science and Engineering, North Carolina State University, Raleigh, North Carolina 27606, USA*

[6]*School of Chemical and Process Engineering, University of Leeds, Leeds, LS2 9JT, UK*

[7]*Department of Materials Science and Engineering, The Pennsylvania State University, University Park, Pennsylvania 16802, USA*

First Author: lmd342@psu.edu

Co-Authors: j.daniels@unsw.edu.au, julia.glaum@ntnu.no, mark.hoffman@unsw.edu.au, hooper.ryanj@gmail.com, goknurtutuncu@gmail.com, forrester.jenny@gmail.com

[*] Corresponding Author: jacobjones@ncsu.edu, Tel: +1-919-515-4557

ABSTRACT

The effect of mechanical stress on the direct piezoelectric properties of pre-poled (1-x)($Na_{0.5}Bi_{0.5}$)TiO_3-x$BaTiO_3$ (NBT-xBT) in the range 4% ≤ x ≤ 13% was studied *in situ* using a mechanical load frame. Prior to mechanical loading, compositions near the morphotropic phase boundary (MPB, x = 6-7% BT) exhibited enhanced ferroelectric and piezoelectric properties compared to compositions further from the MPB. Specifically, the lowest ferroelectric coercive field and highest piezoelectric coefficient within this composition range occurs at x = 7% BT. During mechanical compression, the MPB compositions exhibited the lowest depoling stress. The results demonstrate that, while favorable piezoelectric and ferroelectric properties can be obtained at compositions near the MPB, these compositions are also the most susceptible to the effects of mechanical depoling. Ferroelastic domain wall motion is suggested as the primary factor that may be responsible for these behaviors.

Key Words

Ferroelectric, ferroelastic, morphotropic phase boundary, NBT-BT, mechanical depoling, piezoelectricity

Introduction

Ferroelectric materials are used extensively in sensor and actuator devices due to the piezoelectric properties exhibited [1]. Currently, the most widely used compositions for these applications are based on $Pb(Zr_xTi_{1-x})O_3$ (PZT), due to the wide range of electromechanical coupling and other piezoelectric properties attainable. Recently however, the use of lead-based ceramics has been restricted due to health and environmental concerns [2, 3]. These restrictions have prompted research focusing on Pb-free alternatives. The solid solution $(1-x)(Na_{0.5}Bi_{0.5})TiO_3$-$xBaTiO_3$ (NBT-xBT) has emerged as a candidate among lead-free ferroelectrics, in particular for actuator applications with its relatively high achievable electromechanical coupling factor and mechanical strength [4, 5].

The performance of polycrystalline ferroelectrics is partly evaluated by the piezoelectric properties measured from a poled material [5, 6]. Enhanced piezoelectric properties have been measured in compositions near the morphotropic phase boundary (MPB) for PZT and other ferroelectrics [4, 5, 7, 8]. Prior reports have suggested that the enhanced piezoelectric properties in compositions surrounding the MPB are due, to some extent, to enhanced extrinsic properties, *i.e.* increased domain wall motion (or ferroelectric domain switching) [9]. Additionally, MPB compositions in PZT [10] and NBT-xBT [11] have been observed to exhibit a structurally bridging monoclinic phase as the material transitions from a rhombohedral to tetragonal phase, which may contribute to an increase in octahedral tilting and polarization rotation [12]. These factors can result in an increase in domain wall motion, or domain switching, under the influence of an applied electric field. It is hypothesized that these features are the underlying mechanism for enhanced piezoelectricity [12, 13]. In general, a greater degree of poling and higher piezoelectric performance can be achieved due to increased domain wall motion in compositions near the MPB.

As the domains in these materials are both ferroelectric and ferroelastic, domain walls are not only sensitive to electric field application, but can also be influenced by mechanical stress [14, 15]. Thus, MPB compositions with high ferroelectric domain wall mobility may also exhibit enhanced ferroelastic domain wall motion [16, 17]. Such materials may have a greater tendency to mechanically depole due to loss of domain alignment during the application of mechanical stress [18, 19]. The degradation of the piezoelectric properties due to the ferroelastic behavior of NBT-xBT compositions near the MPB has not yet been fully explored and is the subject of the present study.

In this work, the interplay between the direct piezoelectric d_{33} coefficient of NBT-xBT and applied mechanical stress is reported. The effects of mechanical compression on the d_{33} of NBT-xBT are evaluated for compositions x = 4, 6, 7, 9, and 13%. These compositions are positioned within regions of different crystallographic symmetry in the vicinity of the MPB, which has been reported as 6-7% BT at room temperature [20]. Ferroelectric properties of each composition are determined from polarization and strain measurements. *In situ* compression testing was conducted to analyze the mechanism of depoling as a function of applied stress for all compositions. The results indicate that depoling characteristics in NBT-BT strongly depend on proximity to the MPB.

Experimental

Samples of (1-x)NBT-(x)BT (NBT-xBT), where x = 4, 6, 7, 9, and 13 mol% BT, were prepared by the solid-state reaction of Na_2CO_3 (Alpha Aesar, 99.5%), TiO_2 (Alpha Aesar, 99.6%), Bi_2O_3 (Alpha Aesar, 99.975%), and $BaTiO_3$ (Alpha Aesar, 99.7%). Stoichiometric ratios of the reactant powders were mixed by ball milling in ethanol for 24 h, then these mixtures were dried, ground, and sieved. The powders were calcined for 4 h between 900°C and 1000°C, with the calcining

temperature generally increasing with BT content (temperatures were determined from preliminary phase purity studies). The powders were then ground, sieved, and uniaxially pressed into cylindrical pellets of 6 mm diameter and 15 mm thickness at 690 MPa for 10 min. The pellets were isostatically pressed at 200 MPa for 5 min, and then sintered with surrounding powder of similar composition in a covered crucible for 2 h at 1110°C, 1125°C, 1135°C, 1150°C, and 1150°C for x= 4, 6, 7, 9, and 13%, respectively. The surrounding powder served to compensate for the loss of the volatile cations such as Na and Bi during sintering. The samples were cut into 2 mm thick pellets using a diamond saw. These pellets were then polished with diamond paste (0.5 μm) and annealed at 400°C for 4 h to minimize intergranular stresses induced by the cutting and polishing. Phase purity of the synthesized polycrystalline materials was determined using laboratory X-ray diffraction (Inel 120 CPS Diffractometer; Artenay, France).

Disc-shaped samples of all compositions with thicknesses between 1.55 and 2.79 mm and with ~ 5 mm diameter were used for electrical property characterization. The direct piezoelectric coefficient (d_{33}) was measured for multiple samples of each composition using a Berlincourt d_{33} meter (APC Ceramics, Mackeyville, PA). Dielectric displacement and mechanical displacement were measured in response to electric fields using an aixACCT Ferroelectricity Analyzer (TF Analyzer 2000) with a TREK 20/20C high voltage amplifier. These measurements were used to determine polarization-field and strain-field hysteresis behavior, shown in Fig. 1. An electric field was applied at room temperature to initially unpoled samples with a frequency 0.1 Hz and using a triangular waveform to a maximum of 4.5 kV/mm.

The same samples used for polarization and strain measurements were used in the subsequent mechanical depoling experiments without further exposure to electric fields. Uniaxial compressive mechanical stresses were applied to the pre-poled samples using a BOSE

ElectroForce 3330 Load Frame at a frequency of 0.5 Hz. An initial load of 7.5 MPa was applied to the sample, followed by incremental increases of 15 MPa steps up to a maximum load of 112.5 MPa. To minimize instrument drift and ensure that the load for each stress increment was reached, the initial pre-load (σ_{offset}) was applied to the sample followed by cyclic mechanical loading with an amplitude of 5 MPa ($\Delta\sigma_{cycle}$) which is unipolar relative to σ_{offset}. After a maximum load of $\sigma_{max\ offset}$ = 112.5 MPa was applied, the samples were incrementally unloaded via decreasing the stress by 15 MPa and mechanically cycled at each step. A diagram of the mechanical depoling experiment is outlined in Fig. 2 (a). Figure 2(b) demonstrates the first mechanical loading scheme in which σ_{offset} = 7.5 MPa is applied to the sample, followed by 10 decreasing then increasing cycles of mechanical stress with an amplitude of 5 MPa ($\Delta\sigma_{cycle}$). During each cyclic mechanical loading, the electric charge released from the sample was measured using a charge meter. The d_{33} was determined from the change in measured electric charge of the material during the cyclic mechanical loading as a function of applied mechanical stress.

Results and discussion

Polarization and strain in response to applied bipolar electric fields for samples of each composition are shown in Fig. 1. A change in the hysteresis in both responses is notable as BT concentration changes in NBT-xBT. The highest polarization saturation (Fig. 1 (a)) occurs at x = 7% BT and decreases in compositions further from the MPB. The coercive field amplitude (E_c), the field at which the net polarization is zero, is lowest at x= 7% BT and increases in compositions further from the MPB. It may be inferred from this result, that the MPB is closer to 7% BT than 6% BT. From the polarization-field loops, the E_c for x= 4, 6, 7, 9, and 13% are determined as 3.8, 3.4, 2.1, 2.3, and 2.7 kV/mm, respectively. Additionally, the highest strain saturation (Fig. 1 (b))

occurs at x = 7% BT and decreases in compositions further from the MPB, a trend similar to the polarization at saturation in Fig. 1(a).

In addition to details on the mechanical depoling experiment in Fig. 2(a)-(b), the charge measured during cyclic mechanical loading and the corresponding charge density are shown in Figs. 2(c) and (d), respectively, for NBT-7% BT during the first loading increment. The piezoelectric coefficient (d_{33}) is defined in Fig. 2(c) as the slope of the charge vs. mechanical load curve. The charge density vs. compressive stress hysteresis loops measured during cyclic mechanical loading at the median of the cyclic loading at the initial stress increment (5 MPa) and the median of the cyclic loading at the maximum stress increment (110 MPa) for each composition are shown in Supplemental Fig.1. Decreases in the charge density between the second cycle and the tenth cycle were observed. This decrease was larger at higher stresses compared to lower stresses, shown in the supplemental figure for (5 and 110 MPa). Clamping stresses and creep could have contributed to the decrease in charge density during mechanical depoling. However, the influence of creep would be in addition to the ferroelastic nature of the domain reorientation that occurs during mechanical depoling.

The measured profile of the mechanical depoling sequence is given in Fig. 3(a), and the resulting longitudinal piezoelectric coefficients (d_{33}) as a function of applied compressive stress are exhibited in Figs. 3(b) - (f) for each composition. The compressive stress associated with each d_{33} value represents the median compressive stress of the cycle, i.e. the maximum stress of the cycle subtracted by half the cycle amplitude (2.5 MPa). Therefore, the d_{33} value for the first increment of the loading curve is associated with a compressive stress value of 5 MPa. During loading, a non-linear decrease is observed in the d_{33} values as shown in Figs. 3(b)-(f). The extent of the decrease in d_{33} between two consecutive stress steps may be attributed to the relatively large

stress amplitude applied (5 MPa). Additionally, upon unloading, there is permanent ferroelastic 90º switching caused by the application of a bias stress, a typical characteristic in these classes of ferroelastic materials, such as PZT and $BaTiO_3$ [21, 22, 23, 24]. The absolute changes in the d_{33} values between two consecutive stress steps during loading are also given in Fig. 3. The depoling stress range is then defined as the stress range corresponding to the greatest decrease in d_{33} values during mechanical depoling. The depoling stress range is one way to characterize the range in which domains reorient such that the angle between the applied mechanical stress and the spontaneous strain increases, i.e. non-180º domain reorientation. In this work, the average of the depoling stress range (σ_d) is used to represent the depoling stress for each composition. An average of two data sets for each composition was used to calculate σ_d. The data reveals variations in σ_d with respect to BT content. The lowest σ_d occurs at NBT-7% BT and increases in compositions further from the MPB. This demonstrates that NBT-7% BT requires the lowest stress range to induce ferroelastic domain wall motion.

A comparison of the piezoelectric response (d_{33}), E_c and σ_d for each composition is given in Fig. 4. As previously mentioned, the highest d_{33} was measured in NBT-7% BT and decreased in compositions further from the MPB. These values are in good agreement with the d_{33} values listed by Webber *et al*. for NBT-xBT compositions surrounding the MPB [25]. Both E_c and σ_d follow a similar yet inverse trend to the d_{33} with increasing BT content. Both E_c and σ_d are lowest at NBT-7% BT and increase in compositions further from the MPB. Therefore, although compositions near the MPB exhibit the highest d_{33} and may be poled at a lower electric field, the compositions also undergo mechanical depoling at lower stresses.

It is important to note that the mechanical stress defined in this work is the stress needed to undergo mechanical depoling and can be thought of as the ‘depoling’ stress. The results of the

present study suggest that the stress required to mechanically depole a sample is much lower than the coercive stress values defined in previous literature [25, 26]. This difference could be attributed to variances in grain size, internal strain, defects, processing and poling conditions etc. Additionally, these results suggest that the potential energy barrier that needs to be overcome to pole a sample might be higher than that to depole the same sample. A poled sample contains a higher magnitude of internal microstructural residual stress which can be relieved via mechanical depoling at stresses lower than the coercive stress defined in typical stress-strain studies. Since the samples were pre-poled, i.e. in the ferroelastic phase, prior to mechanical testing, the depoling stress should be distinguished from the mechanical stress reported for a pseudo-cubic to ferroelectric phase transition. The depoling stress range identified in this study is attributed to ferroelastic domain wall motion that occurs after mechanically stressing pre-poled, ferroelectric/ferroelastic phase NBT-xBT. As such, there is a distinct trend in the depoling stress as a function of composition for NBT-xBT. This relationship can be interpreted by considering the amount of BT doping in NBT-xBT. It has been previously observed that enhanced piezoelectric properties are present in compositions at the MPB, x = 6-7% BT, a phenomenon that is attributed to both phase coexistence at the MPB and optimum domain reorientation [27]. From this work, it may be inferred that there is enhanced domain wall motion under applied stresses in x = 6-7% BT and that the effects of extrinsic factors, *i.e.* electric field and mechanical stress, have a greater impact on the piezoelectric properties of MPB compositions.

While there are enhanced piezoelectric properties in compositions closer to the MPB and a greater degree of poling achievable, there is a greater degree of depoling under applied mechanical stress for compositions closer to the MPB. As a result, there is greater degradation of properties under applied mechanical stress for compositions near the MPB with promising piezoelectric

properties. Therefore, it is apparent that there is a property trade off in MPB compositions. Advanced technological devices can make use of the enhanced piezoelectric properties of NBT-xBT compositions near the MPB in applications of low mechanical stresses to minimize depoling and degradation of properties during use. Alternatively, applying a pre-stress to induce depoling has been proven to be beneficial for certain piezoelectric applications. For example, multilayered piezoelectric actuators have been researched for fuel-injection systems in automotive engine applications to utilize a uniaxial compressive pre-stress to enhance the polarization switching upon electric field actuation [28]. The implications of the study in this paper suggest that the level of pre-stress needed to optimize actuation of multilayered piezoelectric actuators can be tuned by varying the composition surrounding the MPB.

Conclusions

In this work, the depoling behavior of compositions in the region of the morphotropic phase boundary in NBT-xBT was examined. Both the E_c and the σ_d range are the lowest at NBT-7% BT and increase in compositions further from the MPB. Although compositions near the MPB exhibit the highest d_{33}, they also undergo mechanical depoling at lower stresses. This suggests that there is enhanced ferroelastic domain switching that occurs in compositions closest to the MPB, which allows for the maximum depoling of these compositions during mechanical testing. These results suggest that there is a strong correlation between compositions within the vicinity of the MPB, enhanced piezoelectric properties and increased domain wall motion. These properties also result in mechanical depoling at lower stresses in MPB compositions.

Acknowledgments

The authors gratefully acknowledge support from the National Science Foundation under award number OISE-1129412 and OISE-1357113, the Australian Research Council under award numbers DP0988182, DP120103968 and DE120102644, the EU call H2020- MSCA-IF-2014 under grant number 655866, and the University of Florida's Ronald E. McNair Post-Baccalaureate Achievement Program under award number P217A120268.

Conflict of Interest: The authors declare no conflict of interest.

References

1. Haertling GH (1999) Ferroelectric Ceramics: History and Technology, J Am Ceram Soc 82:797-818.
2. Jaffe B, Cook WR, Jaffe H (1971) Piezoelectric Ceramics. London: Academic Press, London pp 136.
3. EU-Directive (2003) 2002/96/EC: Restrictions on the Use of Certain Hazardous Substances in Electrical and Electronic Equipment (RoHS). Off J Eur Union 46(L37)19-23.
4. Takenaka T, Maruyama K-I, Sakata K (1991) $(Bi_{1/2}Na_{1/2})TiO_3$-$BaTiO_3$ system for Lead-free piezoelectric ceramics, Jpn J Appl Phys 30(9B):2236-2239.
5. Aksel E, Jones JL (2010) Advances in lead-free piezoelectric materials for sensors and actuators, Sensors 10:1935-1954.
6. Safari A, Akdogan EK (eds). (2008) Piezoelectric and Acoustic Materials for Transducer Applications. Springer, New Jersey.
7. Jaffe B, Roth RS, Marzullo S (1954) Piezoelectric properties of lead zirconate-lead titanate solid-solution ceramics, J Appl Phys 25:809.

8. Shrout TR, Zhang SJ (2007) Lead-free piezoelectric ceramics: Alternatives for PZT?, J Electroceram 19:111-124.
9. Jones JL, Aksel E, Tutuncu G, Usher TM, Chen J, Xing X, Studer AJ (2012) Domain wall and interphase boundary motion in a two-phase morphotropic phase boundary ferroelectric: Frequency dispersion and contribution to piezoelectric and dielectric properties, Phys Rev B 86:024104.
10. Noheda B, Cox DE, Shirane G, Gonzalo JA, Cross LE, Park S-E (1999) A monoclinic ferroelectric phase in the $Pb(Zr_{1-x}Ti_x)O_3$ solid solution, Appl Phys Lett 74:2059.
11. Aksel E, Forrester JS, Jones JL, Thomas PA, Page K, Suchomel MR (2011) Monoclinic crystal structure of polycrystalline $Na_{0.5}Bi_{0.5}TiO_3$, Appl Phys Lett 98:152901.
12. Yao J, Monsegue, N, Murayama M, Leng W, Reynolds WT, Zhang Q, Luo H, Li J-F, Ge W, Viehland D (2012) Role of coexisting tetragonal regions in the rhombohedral phase of $Na_{0.5}Bi_{0.5}TiO_3$-xat.%$BaTiO_3$ crystals on enhanced piezoelectric properties on approaching the morphotropic phase boundary, Appl Phys Lett 100:012901.
13. Damjanovic D (2005) Contributions to the piezoelectric effect in ferroelectric single crystals and ceramics, J Am Ceram Soc 88:2663-2676.
14. Forrester JS, Kisi EH, Studer AJ (2005) Direct observation of ferroelastic domain switching in polycrystalline $BaTiO_3$ using in situ neutron diffraction., J Europ Ceram Soc 25:447-454.
15. Pojprapai(Imlao) S, Luo Z, Clausen B, Vogel SC, Brown DW, Russel J, Hoffman M (2010) Dynamic processes of domain switching in lead zirconate titanate under cyclic mechanical loading by in situ neutron diffraction, Acta Mater 58:1897-1908.

16. Jones JL, Hoffman M, Daniels JE, Studer AJ (2006) Ferroelastic contribution to the piezoelectric response in lead zirconate titanate by in situ stroboscopic neutron diffraction, Physica B 385-386:100-102.

17. Jones JL, Hoffman M, Vogel SC (2007) Ferroelastic domain switching in load zirconate titanate measured by in situ neutron diffraction, Mech Mater 9:283-290.

18. Tai W-P, Kim S-H (1996) Relationship between cyclic loading and degradation of piezoelectric properties in $Pb(Zr,Ti)O_3$ ceramics, Mater Sci Eng B 38:182-185.

19. Zhang QM, Zhao J (1999) Electromechanical properties of lead zirconate titanate piezoceramics under the influence of mechanical stresses, IEEE Trans Ultrason Ferroelectr Freq Control 46:1518-1526.

20. Takenaka T, Maruyama K, Sakata K (1991) $(Bi_{(1/2)}Na_{(1/2)})TiO_3$-$BaTiO_3$ system for lead-free piezoelectric ceramics, Jpn J Appl Phys 30:2236.

21. Berlincourt D and Krueger HHA (1959) Domain processes in lead titanate zirconate and barium titanate ceramics, J Appl Phys 30:11:1804-1810.

22. Krueger HHA and Berlincourt D (1961) Effects of high stress on the piezoelectric properties of transducer materials, J Acoust Soc Am 33:10:1339-1344.

23. Seo Y-H, Franzbach DJ, Koruza J, Bencan A, Malic B, Kosec M, Jones JL, Webber KG (2013) Nonlinear stress-strain behaviour and stress-induced phase transitions in soft $Pb(Zr_{1-x}Ti_x)O_3$ at the morphotropic phase boundary, Phys Rev B 87:094116.

24. Cao H, Evans AG (1993) Nonlinear deformation of ferroelectric ceramics, J Am Ceram Soc 76:890-896.

25. Webber KG, Vogler M, Khansur NH, Kaeswurm B, Daniels JE, Schader FH (2017) Review of the mechanical and fracture behavior of perovskite lead-free ferroelectrics for actuator applications, Smart Mater Struct 26:063001:1-28.

26. Denkhaus SM, Vogler M, Novak N, Rodel J (2017) Short crack fracture toughness in (1-x)($Na_{1/2}Bi_{1/2}$)TiO_3-x$BaTiO_3$ relaxor ferroelectrics, J Am Ceram Soc DOI: 10.1111/jace.15008.

27. Wook J, Daniels JE, Jones JL, Tan X, Thomas PA, Damjanovic D, Rodel J (2011) Evolving morphotropic phase boundary in lead-free ($Bi_{1/2}Na_{1/2}$)TiO_3-$BaTiO_3$ piezoceramics, J Appl Phys 109:014110.

28. Esteves G, Fancher CM, Röhrig S, Maier G, Jones JL, Deluca M (2017) Electric-field-induced structural changes in multi-layer piezoelectric actuators during electrical and mechanical loading, Acta Mater 132:96-105. doi.org/10.1016/j.actamat.2017.04.014.

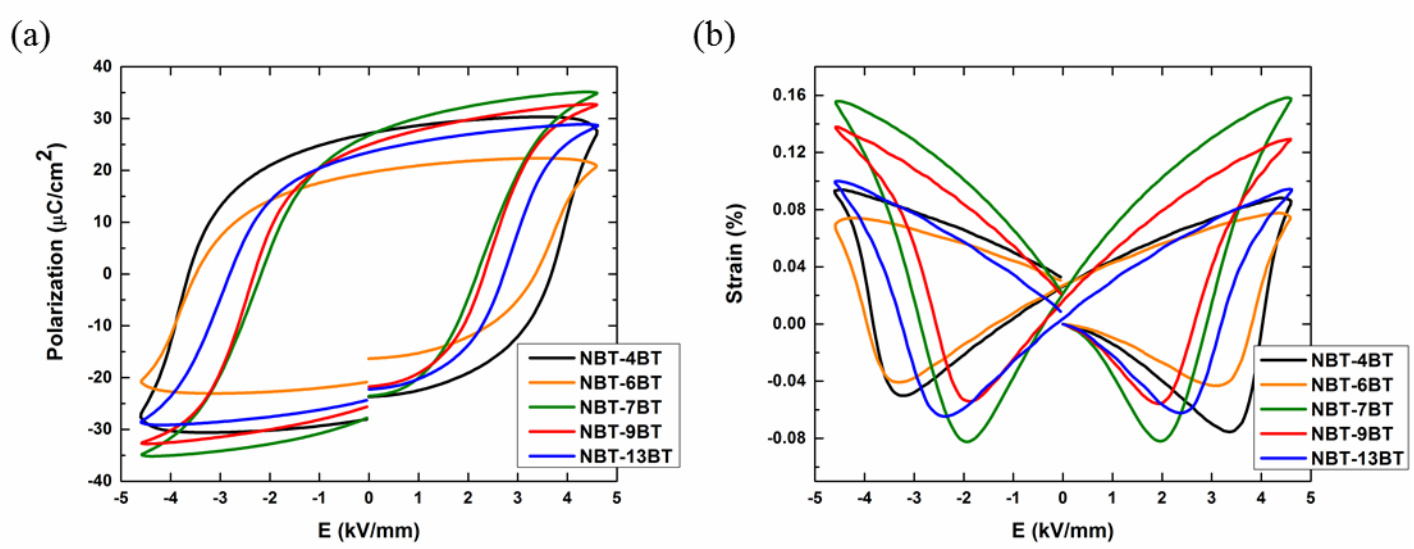

Fig. 1 (a) Polarization, and (b) strain in NBT-xBT compositions as a function of electric field amplitude and composition.

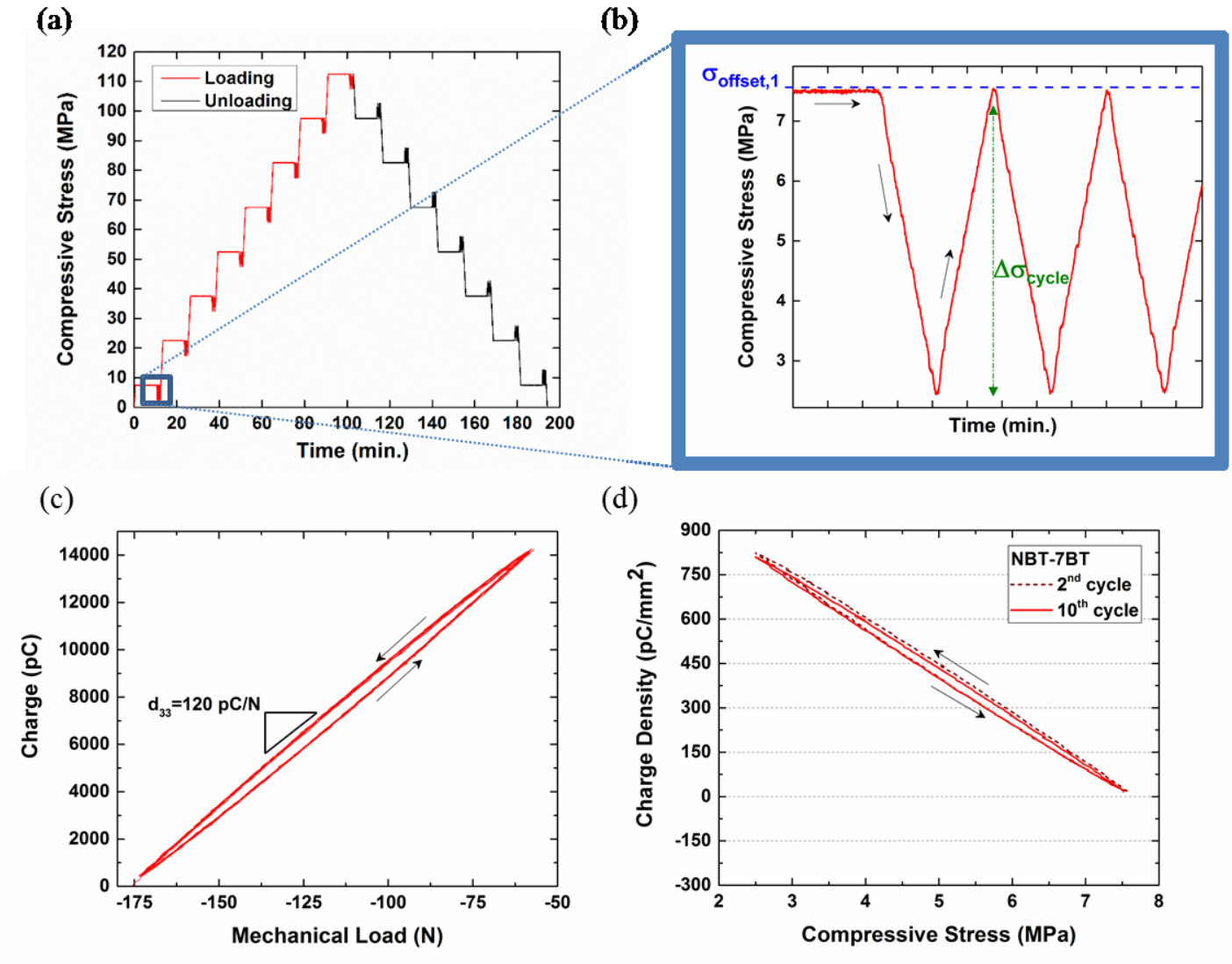

Fig. 2 Details of the mechanical depoling experiment including the mechanical depoling sequence (a), the amplitude of the stress cycle (σ_{cycle}) and stress offset ($\sigma_{offset,1}$) defined for the first loading increment (b). The charge measured during cyclic mechanical loading (c) and corresponding charge density as a function of applied mechanical pressure (d) for NBT-7% BT during the first loading increment are also shown. The piezoelectric coefficient (d_{33}) is defined in figure (c) as the slope of the charge vs. mechanical load curve.

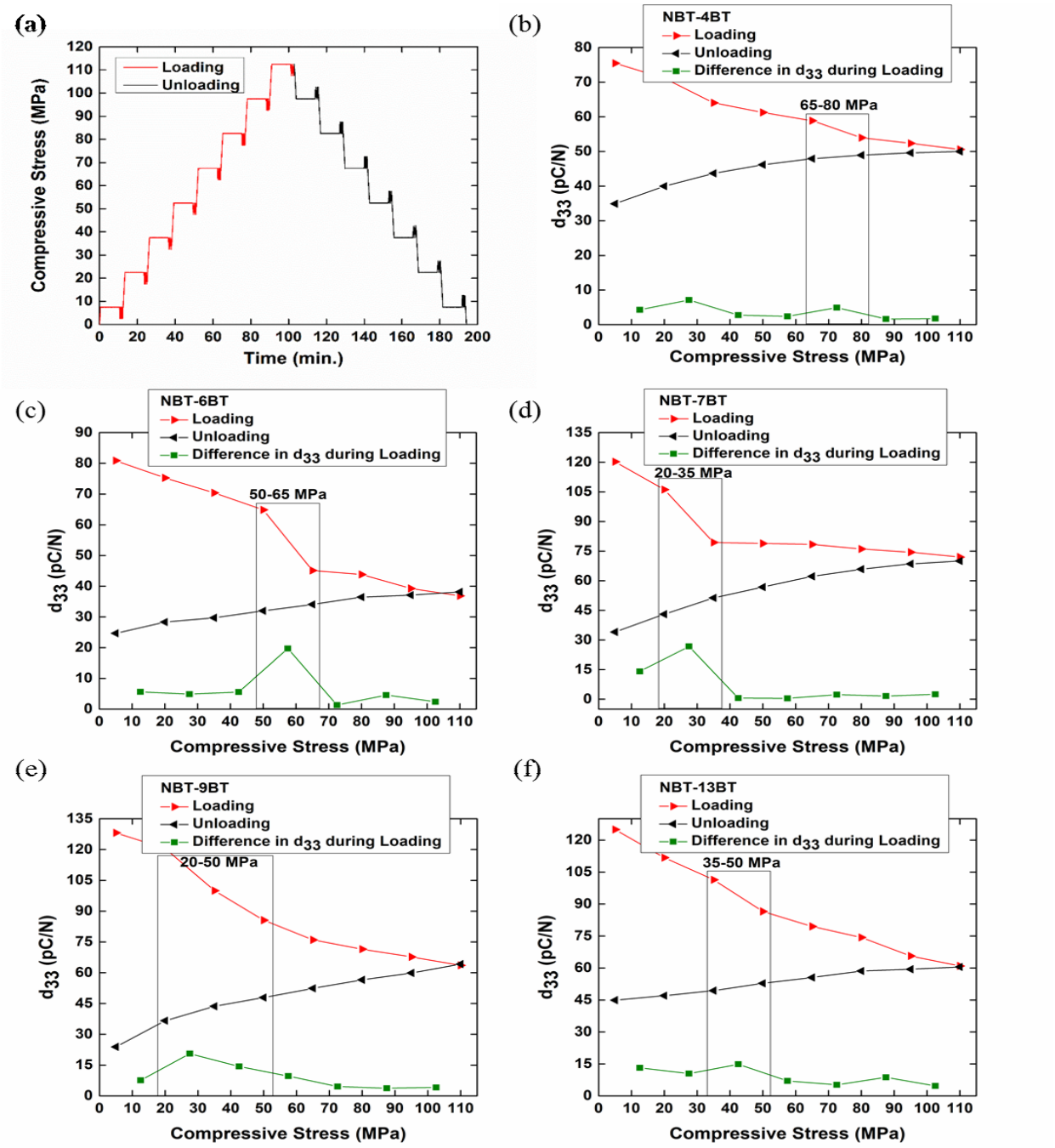

Fig. 3 The mechanical depoling sequence (a) and corresponding graphs of decreasing piezoelectric coefficient (d_{33}) as a function of applied mechanical pressure for (b) NBT-4% BT, (c) NBT-6% BT, (d) NBT-7% BT, (e) NBT-9% BT, and (f) NBT-13% BT. The difference plot below graphs (b)-(f) represent the absolute changes in the d_{33} values between two subsequent steps in the mechanical loading process. The depoling stress range is then defined as the stress range corresponding to the greatest decrease in d_{33} values during mechanical depoling.

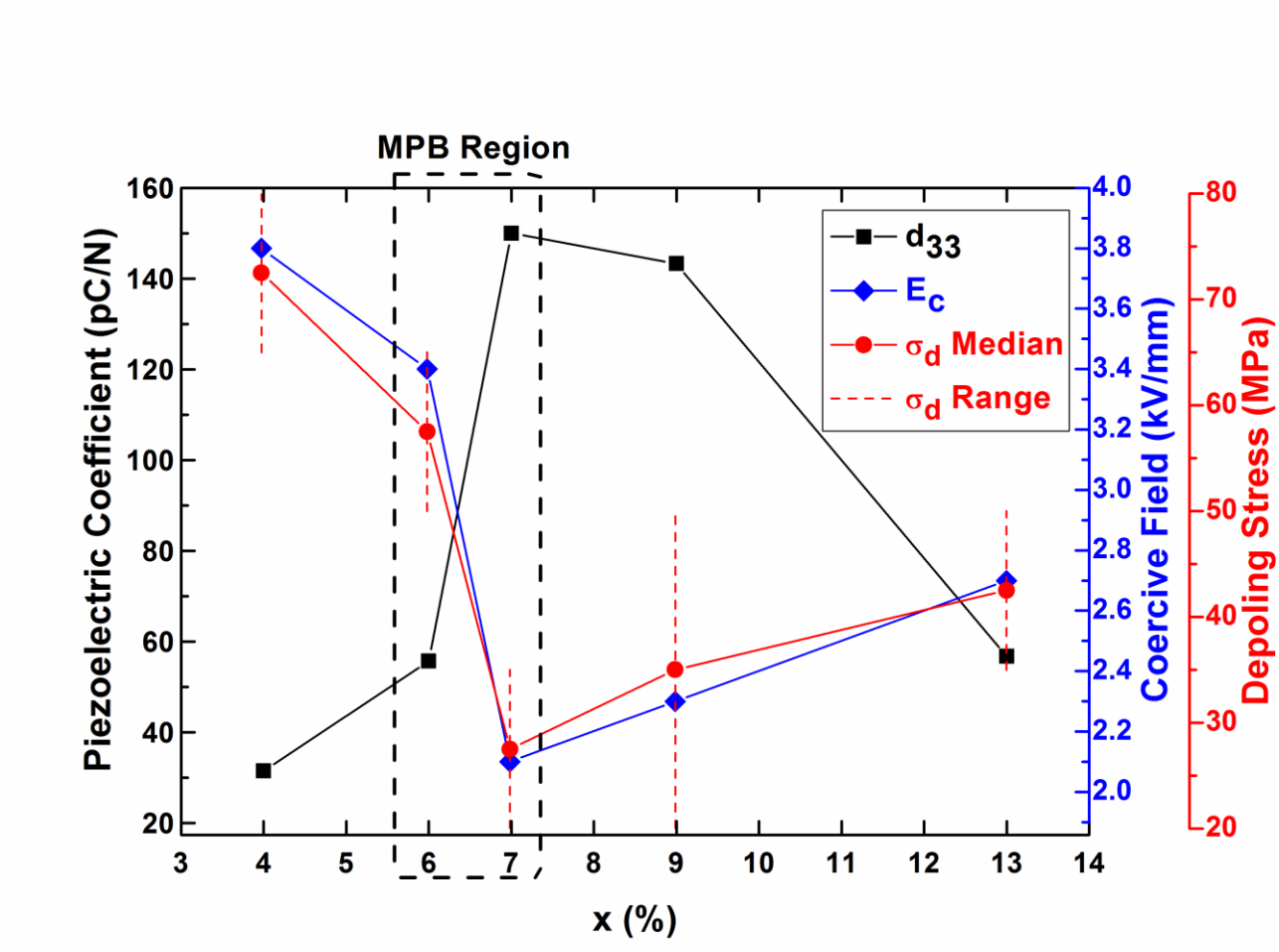

Fig. 4 Initial piezoelectric coefficient (d_{33}), coercive electric field amplitude E_c, depoling stress σ_d (range and median) as a function of composition (x).

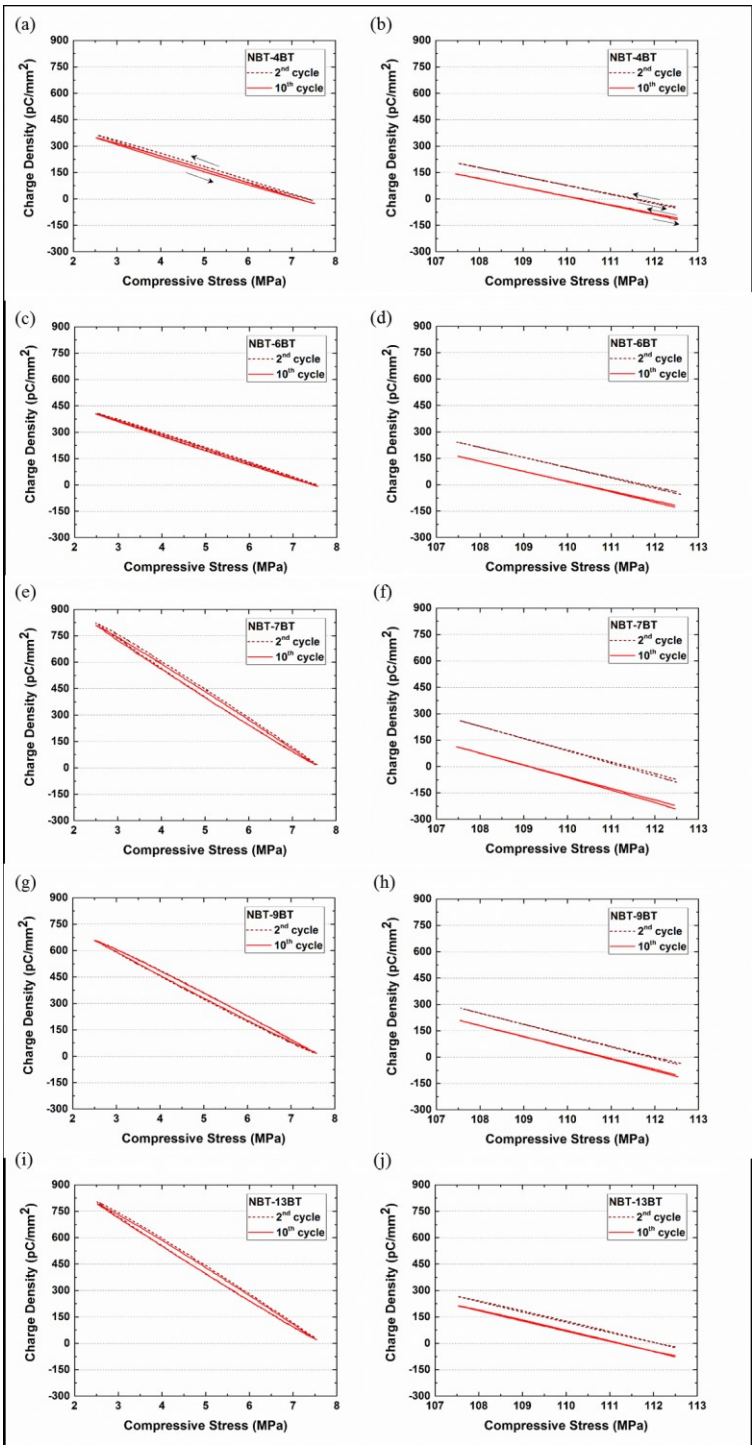

Supplemental Fig. 1 Charge density hysteresis loops during cyclic mechanical loading at the first stress increment (5 MPa) and the maximum stress increment (110 MPa) for (a,b) NBT-4% BT, (c,d) NBT-6% BT, (e,f) NBT-7% BT, (g,h) NBT-9% BT, and (i,j) NBT-13% BT. Charge density vs. compressive stress loops for the 2nd and 10th cycle are plotted for each stress increment and composition.